Interface-enhanced room-temperature Curie temperature in CrPS₄/graphene van der Waals heterostructure

Wenxuan Zhu, Cheng Song [ID],[*] Lei Han, Hua Bai, Chong Chen, and Feng Pan [ID][†]

Key Laboratory of Advanced Materials, School of Materials Science and Engineering, Beijing Innovation Center for Future Chips, Tsinghua University, Beijing 100084, China

Enhancement of the Curie temperature (T_C) has always been a vital problem since the discovery of two-dimensional (2D) van der Waals (vdW) magnets. The interfacial effect from layers with strong spin-orbit coupling (SOC) has been widely investigated to be an effective method. Here, we experimentally show that T_C of vdW CrPS₄ is enhanced from 40 K up to room temperature by the interfacial effect from graphene with weak SOC. The compatible Fermi level between CrPS₄ and graphene enables sufficient interfacial charge transfer across their atomically fine interface, leading to largely elevated T_C of CrPS₄ at the interface without the participation of strong SOC. The enhanced magnetism of CrPS₄ further induces room-temperature exchange splitting in graphene by the magnetic proximity effect, which is shown in the quantum oscillation controlled by field cooling and temperature-dependent resistance. Our work reveals a mechanism for the enhancement of T_C in vdW magnets and the achieved room-temperature all-2D magnetic proximity effect also advances the practical applications of miniaturized low-dissipative 2D spintronics.

Discovery of intrinsic two-dimensional (2D) van der Waals (vdW) magnets provides an ideal platform for spintronic devices with high integration, high performance, and low dissipation [1–4]. The synthesis of 2D vdW magnetic thin flakes has been one of the core targets in the field [5–7], and the recent achievement of intrinsic room-temperature ferromagnetism in few-layer materials definitely advances 2D spintronics towards practical applications [8–11]. Nevertheless, due to the strong dimensionality effect in 2D magnets [12–14], the Curie temperature (T_C) of these novel materials also largely decreases with the thickness. Meanwhile, T_C of most popular vdW magnets is still far below room temperature with the weak exchange coupling, especially for vdW magnetic semiconductors. Therefore, the enhancement of T_C is highly demanded and widely investigated [14–16]. Interfacial effects have proven to be an effective avenue to enhance the ferromagnetism for both traditional magnetic films and vdW magnets [17,18]. It is commonly believed that an adjacent layer with strong spin-orbit coupling (SOC), such as heavy metals and topological insulators, is required to provide a sufficient spin-orbit field, which stabilizes the spin angular momentum and enhances the magnetic anisotropy and T_C [17–22]. However, strong SOC means short spin coherent length, which loses the advantage of 2D vdW magnets and largely increases energy consumption. Therefore, achieving a room-temperature vdW magnet with weak SOC is of vital importance but remains elusive.

T_C in 2D magnets is mainly dominated by two factors, including the strength of exchange coupling and magnetic anisotropy. Fortunately, the enhancement of exchange coupling can be realized by charge transfer, which reconstructs the occupation of electronic structure in 2D magnetic semiconductors and brings about opportunities to elevate T_C without the participation of strong SOC [14,15,23–25]. Both a compatible band structure and a fine interface are required in heterostructures for sufficient charge transfer at the interface, which guarantees effective enhancement on T_C. Here, we propose and experimentally demonstrate the significant enhancement of T_C in an all-2D heterostructure composed of the 2D vdW antiferromagnet CrPS₄ [26–28] and graphene, which benefits from the interfacial charge transfer without strong SOC. As schematically shown by the differential charge density in Fig. 1, the CrPS₄/graphene all-2D vdW heterostructure naturally ensures the atomically fine interface as one of the typical advantages of 2D spintronics, which can cause sufficient charge transfer and orbital hybridization at the interface. Based on first-principles calculations, the Fermi levels of CrPS₄ ($E_F = -3.07$ eV) and graphene ($E_F = -2.89$ eV) are close to each other, enabling the low barrier for charge transfer between them. The significant charge transfer at the interface is also indicated in the density of states of the heterostructure (see Fig. S1 of the Supplemental Material) [29]. Therefore, the additional path of exchange coupling in 2D magnetic semiconductor CrPS₄ could be established through the interfacial charge transfer. T_C of CrPS₄ will thus be largely enhanced through the interfacial effect by graphene with weak SOC. Meanwhile, the Zeeman splitting between spin-up and spin-down Dirac cones in graphene will also be induced via the magnetic proximity effect [30–35] in the CrPS₄/graphene heterostructure. Consequently, the enhanced magnetism of vdW semiconductor CrPS₄ can be characterized by the exchange splitting and ferromagnetism in adjacent

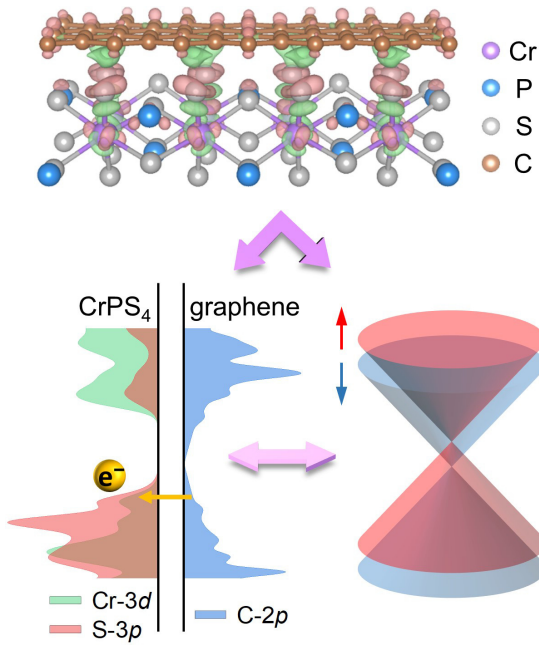[*]songcheng@mail.tsinghua.edu.cn
[†]panf@mail.tsinghua.edu.cn

FIG. 1. Charge transfer and magnetic proximity effect in $CrPS_4$/graphene. In the top panel, red and green isosurface contours indicate charge accumulation and reduction, respectively. The left-bottom panel schematically shows the charge transfer from the density of states of graphene to $CrPS_4$. The overlap of Cr-$3d$ and S-$3p$ orbitals suggests the formation of Cr-S bonds. The right-bottom panel exhibits the band splitting in graphene induced by magnetic proximity effect.

FIG. 2. Characterizations and quantum oscillation of $CrPS_4$/graphene vdW heterostructure. (a) Structural schematics of $CrPS_4$/graphene vdW heterostructure. (b) Raman spectra of bilayer graphene and $CrPS_4$. Fitting of G peak and 2D peak of graphene is shown in green and orange, respectively. Polarized Raman spectra of $CrPS_4$ are exhibited with the polarization of incident light parallel (blue) and perpendicular (red) to the scattered light. (c) Field-dependent longitudinal resistance (R_{xx}) and Hall resistance (R_{xy}) at 10 K. (d) Field-dependent R_{xx} curves at selected temperatures marked in the figure.

graphene. In the following experiments, through the measurements of quantum oscillation controlled by field-cooling [35] and the temperature-dependent resistance in graphene, we report the interfacial-enhanced room-temperature T_C in the $CrPS_4$/graphene all-2D vdW heterostructure.

vdW heterostructures are constructed through the exfoliation of antiferromagnetic insulator $CrPS_4$ flakes on Si/SiO_2 substrate, followed by transferring graphene on them, as schematically shown in Fig. 2(a). Based on the area ratio and the position of G and 2D peaks in the Raman spectrum [36,37] in Fig. 2(b), the graphene is characterized as bilayer. The absence of the D peak around $1350\,cm^{-1}$ indicates the low amount of disorder in graphene [36]. Meanwhile, distinct vibration modes are obtained in Raman spectra of $CrPS_4$ measured with the polarization of incident and scattered light parallel and perpendicular to each other, respectively. The structural symmetry and high quality of $CrPS_4$ flakes is confirmed [38]. Magnetotransport properties of constructed heterostructures were then measured in the $CrPS_4$/graphene Hall devices (Fig. S2) [29]. Concomitant data are illustrated in Fig. 2(c). Clear quantum oscillation, including Shubnikov–de Haas (SdH) in longitudinal resistance (R_{xx}) and quantum Hall oscillation in Hall resistance (R_{xy}), is observed above 20 kOe during an out-of-plane field scanning at 10 K. Due to the little contribution from insulating $CrPS_4$ [26] on the electrical signal, the quantum oscillation reveals the Landau levels in graphene and can characterize the exchange splitting induced by the magnetic proximity effect. Consequently, the magnetism of adjacent $CrPS_4$ is reflected. With the increase
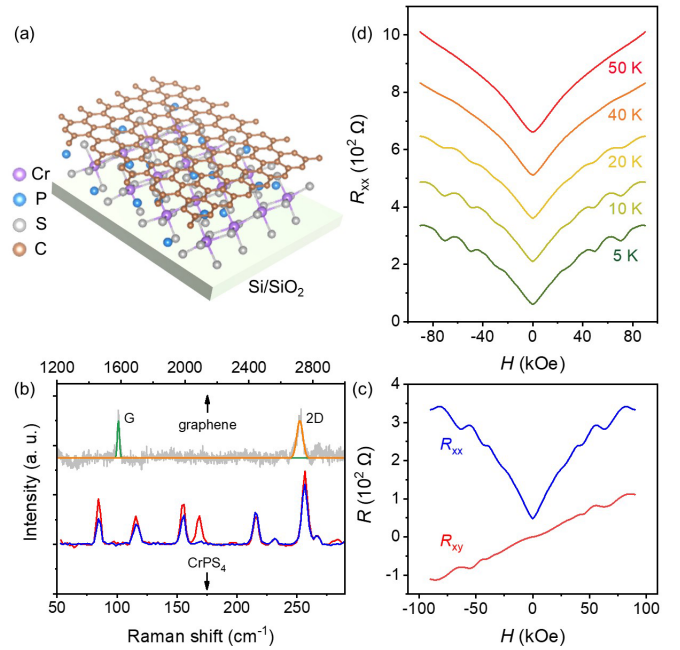
of temperature, the quantum oscillation gradually blurs and vanishes beyond 40 K in Fig. 2(d), which shows the intrinsic attenuation of quantum effects with enhanced thermal fluctuation. The following measurements were performed at 10 K and zero gate voltage to characterize the quantum oscillations without special remarks.

First, to demonstrate the exchange splitting in graphene induced by the magnetic proximity effect, field-cooling processes were carried out, which can control the magnetism of adjacent $CrPS_4$ above its magnetic ordering temperature. Consequently, the induced splitting energy will be simultaneously modulated, which results in the shift of Landau levels and quantum oscillation [35]. Therefore, the change of quantum oscillations measured at 10 K can be observed. As presented in Fig. 3(a), quantum oscillation in R_{xy} can be controlled by field cooling, demonstrating the emergent exchange splitting in graphene by adjacent $CrPS_4$. After field cooling, the magnetic fields where quantum oscillation emerges obviously deviate from the state of zero field cooling (ZFC), illustrating the change of splitting energy and Landau levels in graphene. This control is volatile, which can be eliminated after ZFC as shown in Fig. S3(a) [29]. Meanwhile, the field cooling with opposite magnetic field exhibits a similar modulation in Fig. S3(b) [29]. In contrast, field cooling shows no control on the transport in pristine graphene (Fig. S4) [29], which further supports the existence of the magnetic proximity effect. More surprisingly, almost no change of quantum oscillation is
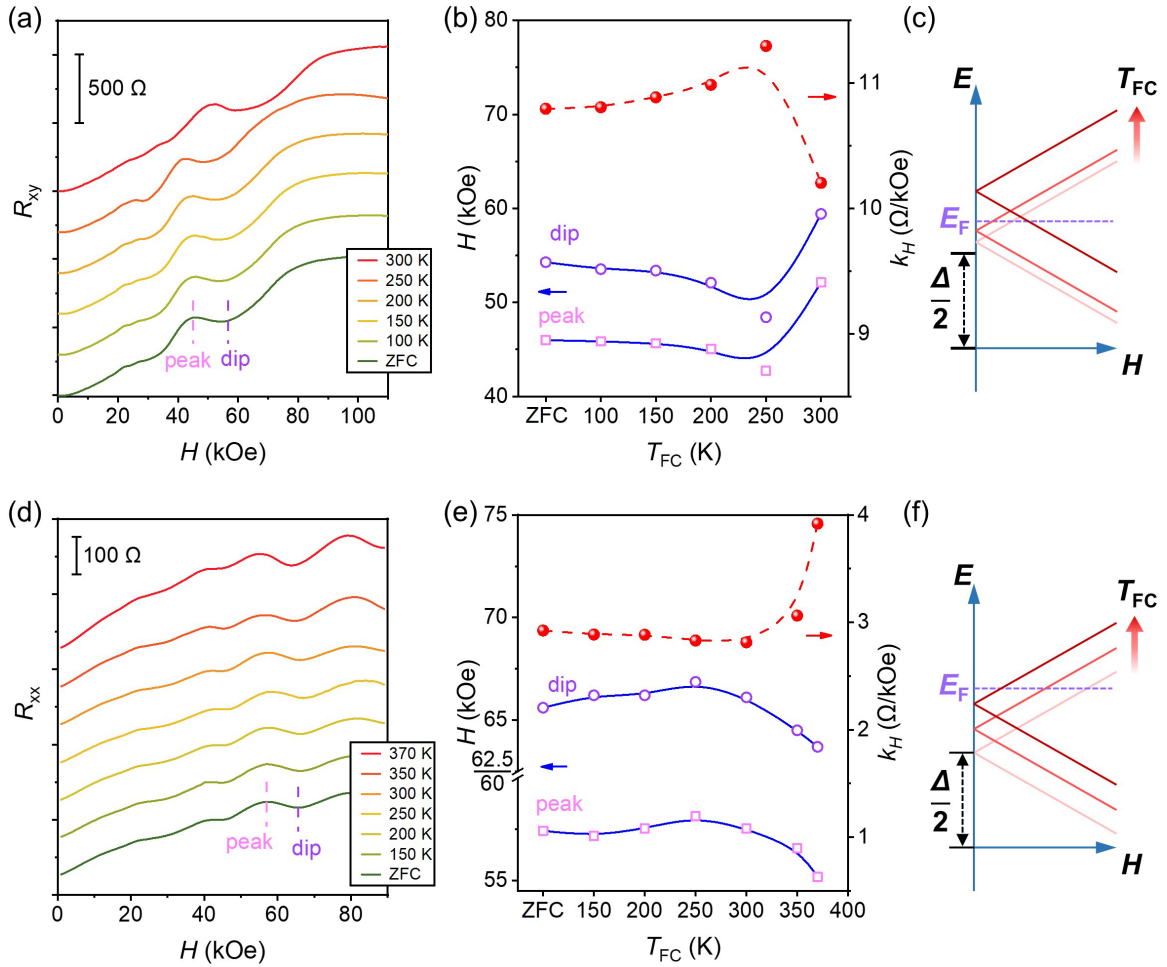
FIG. 3. Quantum oscillation and Landau levels controlled by field cooling. (a) Field-dependent R_{xy} measured at 10 K controlled by field cooling at different temperature. (b) Extracted field of quantum oscillation around 50 kOe and the linear slop of ordinary Hall resistance background (k_H) from (a). (c) Schematic of Landau level spectrum with increasing temperature of field cooling (T_{FC}) corresponding to (a), (b). (d) Field-dependent R_{xx} measured at 10 K controlled by field cooling at different temperature. (e) Extracted field of quantum oscillation around 60 kOe and the linear slope of ordinary Hall resistance background (k_H) from (d). (f) Schematic of Landau level spectrum with increasing T_{FC} corresponding to (d), (e).

observed between ZFC and the relatively low temperature of field cooling (T_{FC}), such as 150 K, in Fig. 3(a). The obvious modulation occurs until T_{FC} further reaches 250 K, which is much higher than the magnetic ordering temperature of pristine bulk $CrPS_4$ around 40 K.

The magnetic fields of the quantum oscillation around 50 kOe with different T_{FC} are then extracted from Fig. 3(a) and summarized in Fig. 3(b). Considering the background of the ordinary Hall effect and magnetoresistance in R_{xy}, positions of maxima (peak) and minima (dip) are obtained by zeros in differential curves for better accuracy (Fig. S5) [29]. Corresponding linear slopes (k_H) of the ordinary Hall resistance background, which possesses negative correlation with the carrier concentration and can characterize the band structure of graphene, are also exhibited. Figure 3(b) clearly verifies that the obvious shift of quantum oscillation only appears until critical T_{FC} around 250 K. Meanwhile, k_H shows an opposite trend and the same critical T_{FC} with the position of quantum oscillation. The shift of quantum oscillation to a higher field suggests a larger oscillation frequency (B_f) [39], and the carrier concentration shows a positive correlation with B_f, which

is consistent with the pristine graphene and other systems with the proximity effect [32,39,40]. The results are also further supported by the measurements of R_{xx} with a higher critical T_{FC} around 300 K, which is demonstrated by Figs. 3(d) and 3(e).

Note that the shift trend of quantum oscillation displayed in Figs. 3(b) and 3(e) is opposite, which is attributed to different locations of E_F relative to the Dirac cone among devices. The corresponding schematic Landau level spectra are illustrated in Figs. 3(c) and 3(f), respectively. The aligned magnetic moments by field cooling enhance the splitting energy Δ in graphene with increasing T_{FC} above T_C, leading to the lift of the spin-up Dirac cone and Landau levels. In Fig. 3(c), E_F passes the Dirac point during the gradual increase of Δ and the magnetic field of crossing consequently shows a first slight decrease with $T_{FC} = 250$ K followed by the increase with $T_{FC} = 300$ K, which is confirmed by the results shown in Figs. 3(a) and 3(b). In contrast, in Fig. 3(f), the upper shift of the Dirac cone leads to the crossing between E_F and the Landau level at lower magnetic fields monotonically, exhibiting a different trend with Fig. 3(c).
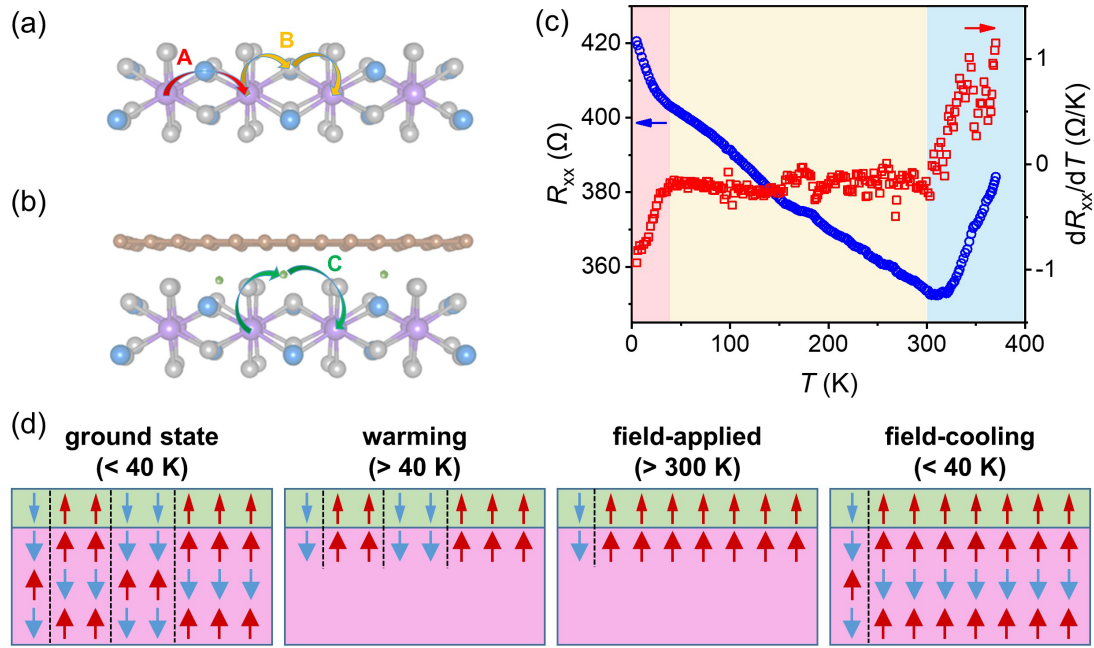
FIG. 4. Schematic of exchange coupling in (a) $CrPS_4$ and (b) $CrPS_4$/graphene heterostructure. (c) Temperature-dependent R_{xx} and its derivative (dR_{xx}/dT) with 50 kOe field applied. (d) Evolution process of magnetic configuration controlled by field-cooling in $CrPS_4$/graphene.

Based on the common understanding, field cooling is able to effectively control the magnetism above the magnetic ordering temperature in ferromagnets or antiferromagnets, especially with uncompensated moments, such as noncolinear antiferromagnets [35] or A-type layered antiferromagnets. Accordingly, the exchange splitting in adjacent graphene induced by the magnetic proximity effect can be modulated. Therefore, the controllable magnetic proximity effect by field cooling indicates the existence of net ferromagnetism in adjacent $CrPS_4$ at the interface and the critical T_{FC} reflects its T_C. Based on the observation of T_{FC} around 300 K, the existence of a higher critical temperature of magnetic ordering up to room temperature is revealed in $CrPS_4$ with the construction of heterostructures with graphene. The interfacial charge transfer due to orbital hybridizations reconstructs the electron occupation and elevates T_C of the $CrPS_4$ layer adjacent to the interface. The first-principles calculations theoretically prove the promoted energy of magnetic anisotropy (from 0.02 to 3 meV/Cr) in $CrPS_4$ after being constructed into heterostructures with graphene, indicating enhanced T_C. In addition, in 2D magnets, the strength of exchange coupling participates in the decision of T_C [1]. In semiconductor $CrPS_4$ with poor conductivity, the exchange coupling is mainly directly established between Cr atoms and indirectly mediated by intermediate anions, as schematically shown in Fig. 4(a). After being constructed into a heterostructure with graphene, the carrier density in $CrPS_4$ increased with the interfacial charge transfer, which is indicated by the vanishing band gap in the density of states exhibited in Fig. S1 [29]. As shown in Fig. 4(b), the additional path of exchange coupling in $CrPS_4$/graphene is indirectly established through the conduction electrons. Therefore, the increased carrier enhances the exchange coupling, which changes from 3 to 19 meV/Cr according to the calculations, and consequently largely elevates T_C.

Besides the quantum oscillation, the transitions between different magnetic configurations also appear in the measurement of temperature-dependent resistance [35,41], which illustrates the magnetic phase diagram and further supports the largely enhanced T_C in $CrPS_4$/graphene. Compared to the semiconductor property of pristine graphene in Fig. S6 [29], two obvious kinks appear in the temperature-dependent R_{xx} of $CrPS_4$/graphene and its derivative (dR_{xx}/dT) as highlighted in Fig. 4(c), which indicates two transitions. One appears around 40 K with the other above 300 K, corresponding to the magnetic ordering temperature of pristine bulk $CrPS_4$ and T_C of enhanced interfacial $CrPS_4$, respectively. We can now visualize the complete evolution process of $CrPS_4$/graphene heterostructure during the field cooling, as schematically shown in Fig. 4(d). In the ground state, $CrPS_4$ possesses bulk A-type antiferromagnetism with exchange splitting and ferromagnetism induced in the graphene layer according to the interfacial $CrPS_4$ layer via the magnetic proximity effect. With warming above the magnetic ordering temperature of pristine $CrPS_4$ ($\sim$40 K), the bulk magnetism vanishes with the enhanced ferromagnetism persisting in the interfacial $CrPS_4$ layer due to the charge transfer. Consequently, the field cooling at this temperature range still shows little modulation on either the magnetism of $CrPS_4$ or the exchange splitting of graphene. After further warming up above enhanced T_C of $CrPS_4$ (around 300 K), magnetic moments will be aligned by an applied magnetic field, which results in the simultaneous modulation of the exchange splitting induced in graphene. By field cooling, the bulk antiferromagnetism of $CrPS_4$ will be arranged according to the interfacial $CrPS_4$ layer. With the increase of magnetic field applied during field cooling, the splitting energy and the corresponding shift in quantum oscillation is promoted and gradually saturates, suggesting the saturation of aligned interfacial magnetic moments (Fig. S7) [29]. The results above illuminate the magnetic

phase transitions in $CrPS_4$/graphene vdW heterostructure separated by two critical magnetic ordering temperatures, which are the transition from bulk antiferromagnetism to interfacial ferromagnetism around 40 K followed by the transition from interfacial ferromagnetism to paramagnetism around 300 K.

In conclusion, we have experimentally reported the room-temperature T_C in $CrPS_4$/graphene all-2D heterostructure as the result of interfacial charge transfer without strong SOC, which is characterized by the exchange splitting and ferromagnetism in graphene induced by the magnetic proximity effect. Our work puts forward an alternative perspective for the elevation of T_C in 2D vdW magnets, which could promote 2D spintronics for practical applications.

Furthermore, the room-temperature proximity effect observed in $CrPS_4$/graphene heterostructure also breaks the bottleneck of low temperature in the all-2D proximity effect, which unprecedentedly advances the microminiaturization of graphene-based multifunctional spintronic devices [32,23]. Therefore, the realization of room-temperature controllable spin transport with long distance and low dissipation is highly expected.

[1] C. Gong and X. Zhang, Two-dimensional magnetic crystals and emergent heterostructure devices, Science **363**, eaav4450 (2019).

[2] M. Gibertini, M. Koperski, A. F. Morpurgo, and K. S. Novoselov, Magnetic 2D materials and heterostructures, Nat. Nanotechnol. **14**, 408 (2019).

[3] H. Li, S. Ruan, and Y. J. Zeng, Intrinsic van der waals magnetic materials from bulk to the 2D limit: new frontiers of spintronics, Adv. Mater. **31**, 1900065 (2019).

[4] B. Huang, M. A. McGuire, A. F. May, D. Xiao, P. Jarillo-Herrero, and X. Xu, Emergent phenomena and proximity effects in two-dimensional magnets and heterostructures, Nat. Mater. **19**, 1276 (2020).

[5] L. Meng, Z. Zhou, M. Xu, S. Yang, K. Si, L. Liu, X. Wang, H. Jiang, B. Li, P. Qin, P. Zhang, J. Wang, Z. Liu, P. Tang, Y. Ye, W. Zhou, L. Bao, H. J. Gao, and Y. Gong, Anomalous thickness dependence of curie temperature in air-stable two-dimensional ferromagnetic 1T-CrTe₂ grown by chemical vapor deposition, Nat. Commun. **12**, 809 (2021).

[6] M. Bian, L. Zhu, X. Wang, J. Choi, R. V. Chopdekar, S. Wei, L. Wu, C. Huai, A. Marga, Q. Yang, Y. C. Li, F. Yao, T. Yu, S. A. Crooker, X. M. Cheng, R. F. Sabirianov, S. Zhang, J. Lin, Y. Hou, and H. Zeng, Dative epitaxy of commensurate monocrystalline covalent van der waals moiré supercrystal, Adv. Mater. **34**, 2200117 (2022).

[7] B. Zhang, C. Yun, H. Wu, Z. Zhao, Y. Zeng, D. Liang, T. Shen, J. Zhang, X. Huang, J. Song, J. Xu, Q. Zhang, P. H. Tan, S. Gao, and Y. Hou, Two-dimensional wedge-shaped magnetic eus: insight into the substrate step-guided epitaxial synthesis on sapphire, J. Am. Chem. Soc. **144**, 19758 (2022).

[8] X. Sun, W. Li, X. Wang, Q. Sui, T. Zhang, Z. Wang, L. Liu, D. Li, S. Feng, S. Zhong, H. Wang, V. Bouchiat, M. Nunez Regueiro, N. Rougemaille, J. Coraux, A. Purbawati, A. Hadj-Azzem, Z. Wang, B. Dong, X. Wu, T. Yang, G. Yu, B. Wang, Z. Han, X. Han, and Z. Zhang, Room temperature ferromagnetism in ultra-thin van der waals crystals of 1T-CrTe₂, Nano Res. **13**, 3358 (2020).

[9] X. Zhang, Q. Lu, W. Liu, W. Niu, J. Sun, J. Cook, M. Vaninger, P. F. Miceli, D. J. Singh, S. W. Lian, T. R. Chang, X. He, J. Du, L. He, R. Zhang, G. Bian, and Y. Xu, Room-temperature intrinsic ferromagnetism in epitaxial CrTe₂ ultrathin films, Nat. Commun. **12**, 2492 (2021).

[10] G. Zhang, F. Guo, H. Wu, X. Wen, L. Yang, W. Jin, W. Zhang, and H. Chang, Above-room-temperature strong intrinsic ferromagnetism in 2D van der waals Fe₃GaTe₂ with large perpendicular magnetic anisotropy, Nat. Commun. **13**, 5067 (2022).

[11] W. Zhu, C. Song, Q. Wang, H. Bai, S. Yin, and F. Pan, Anomalous displacement reaction for synthesizing above-room-temperature and air-stable VdW ferromagnet PtTe₂Ge₁/₃, Natl. Sci. Rev. **10**, nwac173 (2023).

[12] C. Gong, L. Li, Z. Li, H. Ji, A. Stern, Y. Xia, T. Cao, W. Bao, C. Wang, Y. Wang, Z. Q. Qiu, R. J. Cava, S. G. Louie, J. Xia, and X. Zhang, Discovery of intrinsic ferromagnetism in two-dimensional van der waals crystals, Nature (London) **546**, 265 (2017).

[13] B. Huang, G. Clark, E. Navarro-Moratalla, D. R. Klein, R. Cheng, K. L. Seyler, D. Zhong, E. Schmidgall, M. A. McGuire, D. H. Cobden, W. Yao, D. Xiao, P. Jarillo-Herrero, and X. Xu, Layer-dependent ferromagnetism in a van der waals crystal down to the monolayer limit, Nature (London) **546**, 270 (2017).

[14] Y. Deng, Y. Yu, Y. Song, J. Zhang, N. Z. Wang, Z. Sun, Y. Yi, Y. Z. Wu, S. Wu, J. Zhu, J. Wang, X. H. Chen, and Y. Zhang, Gate-tunable room-temperature ferromagnetism in two-dimensional Fe₃GeTe₂, Nature (London) **563**, 94 (2018).

[15] I. A. Verzhbitskiy, H. Kurebayashi, H. Cheng, J. Zhou, S. Khan, Y. P. Feng, and G. Eda, Controlling the magnetic anisotropy in Cr₂Ge₂Te₆ by electrostatic gating, Nat. Electron. **3**, 460 (2020).

[16] X. Jiang, Q. Liu, J. Xing, N. Liu, Y. Guo, Z. Liu, and J. Zhao, Recent progress on 2D magnets: fundamental mechanism, structural design and modification, Appl. Phys. Rev. **8**, 031305 (2021).

[17] H. Wang, Y. Liu, P. Wu, W. Hou, Y. Jiang, X. Li, C. Pandey, D. Chen, Q. Yang, H. Wang, D. Wei, N. Lei, W. Kang, L. Wen, T. Nie, W. Zhao, and K. L. Wang, Above room-temperature ferromagnetism in wafer-scale two-dimensional van der waals Fe₃GeTe₂ tailored by a topological insulator, ACS Nano **14**, 10045 (2020).

[18] W. Zhu, C. Song, L. Han, H. Bai, Q. Wang, S. Yin, L. Huang, T. Chen, and F. Pan, Interface-enhanced ferromagnetism with long-distance effect in van der waals semiconductor, Adv. Funct. Mater. **32**, 2108953 (2022).

[19] X. Chen, H. Wang, H. Liu, C. Wang, G. Wei, C. Fang, H. Wang, C. Geng, S. Liu, P. Li, H. Yu, W. Zhao, J. Miao, Y. Li,

L. Wang, T. Nie, J. Zhao, and X. Wu, Generation and control of terahertz spin currents in topology-induced 2D ferromagnetic Fe$_3$GeTe$_2$|Bi$_2$Te$_3$ heterostructures, Adv. Mater. **34**, 2106172 (2022).

[20] F. Katmis, V. Lauter, F. S. Nogueira, B. A. Assaf, M. E. Jamer, P. Wei, B. Satpati, J. W. Freeland, I. Eremin, D. Heiman, P. Jarillo-Herrero, and J. S. Moodera, A high-temperature ferromagnetic topological insulating phase by proximity coupling, Nature (London) **533**, 513 (2016).

[21] J. Kim, K. W. Kim, H. Wang, J. Sinova, and R. Wu, Understanding the Giant Enhancement of Exchange Interaction in Bi$_2$Se$_3$-Eus Heterostructures, Phys. Rev. Lett. **119**, 027201 (2017).

[22] X. J. Dong, J. Y. You, Z. Zhang, B. Gu, and G. Su, Great enhancement of curie temperature and magnetic anisotropy in two-dimensional van der waals magnetic semiconductor heterostructures, Phys. Rev. B **102**, 144443 (2020).

[23] W. Zhuo, B. Lei, S. Wu, F. Yu, C. Zhu, J. Cui, Z. Sun, D. Ma, M. Shi, H. Wang, W. Wang, T. Wu, J. Ying, S. Wu, Z. Wang, and X. Chen, Manipulating ferromagnetism in few-layered Cr$_2$Ge$_2$Te$_6$, Adv. Mater. **33**, 2008586 (2021).

[24] M. Keunecke, F. Lyzwa, D. Schwarzbach, V. Roddatis, N. Gauquelin, K. Müller-Caspary, J. Verbeeck, S. J. Cal, F. Klose, M. Jungbauer, and V. Moshnyaga, High-T_C interfacial ferromagnetism in SrMnO$_3$/LaMnO$_3$ superlattices, Adv. Funct. Mater. **30**, 1808270 (2020).

[25] Z. Li, X. Chen, Y. Chen, Q. Zhang, H. Zhang, J. Zhang, W. Shi, B. He, J. Zhang, J. Song, F. Han, B. Liu, L. Gu, F. Hu, Y. Chen, B. Shen, and J. Sun, Infinite-layer/perovskite oxide heterostructure-induced high-spin states in SrCuO$_2$/SrRuO$_3$ bilayer films, Mater. Horizons **8**, 3468 (2021).

[26] Y. Peng, S. Ding, M. Cheng, Q. Hu, J. Yang, F. Wang, M. Xue, Z. Liu, Z. Lin, M. Avdeev, Y. Hou, W. Yang, Y. Zheng, and J. Yang, Magnetic structure and metamagnetic transitions in the van der waals antiferromagnet CrPS$_4$, Adv. Mater. **32**, 2001200 (2020).

[27] P. Gu, Q. Tan, Y. Wan, Z. Li, Y. Peng, J. Lai, J. Ma, X. Yao, S. Yang, K. Yuan, D. Sun, B. Peng, J. Zhang, and Y. Ye, Photoluminescent quantum interference in a van der waals magnet preserved by symmetry breaking, ACS Nano **14**, 1003 (2020).

[28] J. Son, S. Son, P. Park, M. Kim, Z. Tao, J. Oh, T. Lee, S. Lee, J. Kim, K. Zhang, K. Cho, T. Kamiyama, J. H. Lee, K. F. Mak, J. Shan, M. Kim, J. G. Park, and J. Lee, Air-stable and layer-dependent ferromagnetism in atomically thin van der waals CrPS$_4$, ACS Nano **15**, 16904 (2021).

[29] See Supplemental Material at http://link.aps.org/supplemental/10.1103/PhysRevB.108.L100406 for a detailed description of sample characterization, device fabrication, first-principles calculations, and transport measurements, which includes Refs. [42–49].

[30] H. X. Yang, A. Hallal, D. Terrade, X. Waintal, S. Roche, and M. Chshiev, Proximity Effects Induced in Graphene by Magnetic Insulators: First-Principles Calculations on Spin Filtering and Exchange-Splitting Gaps, Phys. Rev. Lett. **110**, 046603 (2013).

[31] Z. Wang, C. Tang, R. Sachs, Y. Barlas, and J. Shi, Proximity-Induced Ferromagnetism in Graphene Revealed by the Anomalous Hall Effect, Phys. Rev. Lett. **114**, 016603 (2015).

[32] P. Wei, S. Lee, F. Lemaitre, L. Pinel, D. Cutaia, W. Cha, F. Katmis, Y. Zhu, D. Heiman, J. Hone, J. S. Moodera, and C. T. Chen, Strong interfacial exchange field in the graphene/eus heterostructure, Nat. Mater. **15**, 711 (2016).

[33] C. Tang, Z. Zhang, S. Lai, Q. Tan, and W. bo Gao, Magnetic proximity effect in Graphene/CrBr$_3$ van der waals heterostructures, Adv. Mater. **32**, 1908498 (2020).

[34] T. S. Ghiasi, A. A. Kaverzin, A. H. Dismukes, D. K. de Wal, X. Roy, and B. J. van Wees, Electrical and thermal generation of spin currents by magnetic bilayer graphene, Nat. Nanotechnol. **16**, 788 (2021).

[35] Y. Wu, G. Yin, L. Pan, A. J. Grutter, Q. Pan, A. Lee, D. A. Gilbert, J. A. Borchers, W. Ratcliff, A. Li, X. dong Han, and K. L. Wang, Large exchange splitting in monolayer graphene magnetized by an antiferromagnet, Nat. Electron. **3**, 604 (2020).

[36] A. C. Ferrari, J. C. Meyer, V. Scardaci, C. Casiraghi, M. Lazzeri, F. Mauri, S. Piscanec, D. Jiang, K. S. Novoselov, S. Roth, and A. K. Geim, Raman Spectrum of Graphene and Graphene Layers, Phys. Rev. Lett. **97**, 187401 (2006).

[37] D. Graf, F. Molitor, K. Ensslin, C. Stampfer, A. Jungen, C. Hierold, and L. Wirtz, Spatially resolved raman spectroscopy of single- and few-layer graphene, Nano Lett. **7**, 238 (2007).

[38] S. Kim, J. Lee, C. Lee, and S. Ryu, Polarized raman spectra and complex raman tensors of antiferromagnetic semiconductor CrPS$_4$, J. Phys. Chem. C **125**, 2691 (2021).

[39] B. Zhou, J. Balgley, P. Lampen-Kelley, J. Q. Yan, D. G. Mandrus, and E. A. Henriksen, Evidence for charge transfer and proximate magnetism in graphene- α-RuCl$_3$ heterostructures, Phys. Rev. B **100**, 165426 (2019).

[40] Y. Zhang, Y. W. Tan, H. L. Stormer, and P. Kim, Experimental observation of the quantum hall effect and berry's phase in graphene, Nature (London) **438**, 201 (2005).

[41] D. V. Averyanov, I. S. Sokolov, A. M. Tokmachev, O. E. Parfenov, I. A. Karateev, A. N. Taldenkov, and V. G. Storchak, High-temperature magnetism in graphene induced by proximity to EuO, ACS Appl. Mater. Interfaces **10**, 20767 (2018).

[42] G. Kresse and J. Furthmüller, Efficiency of ab-initio total energy calculations for metals and semiconductors using a plane-wave basis set, Comput. Mater. Sci. **6**, 15 (1996).

[43] G. Kresse and J. Furthmüller, Efficient iterative schemes for ab initio total-energy calculations using a plane-wave basis set, Phys. Rev. B **54**, 11169 (1996).

[44] P. E. Blöchl, Projector augmented-wave method, Phys. Rev. B **50**, 17953 (1994).

[45] G. Kresse and D. Joubert, From ultrasoft pseudopotentials to the projector augmented-wave method, Phys. Rev. B **59**, 1758 (1999).

[46] J. P. Perdew, K. Burke, and M. Ernzerhof, Generalized Gradient Approximation Made Simple, Phys. Rev. Lett. **77**, 3865 (1996).

[47] S. Grimme, J. Antony, S. Ehrlich, and H. Krieg, A consistent and accurate ab initio parametrization of density functional dispersion correction (DFT-D) for the 94 elements H-Pu, J. Chem. Phys. **132**, 154104 (2010).

[48] M. Joe, J. Lee, and C. Lee, Dominant in-plane cleavage direction of CrPS$_4$, Comput. Mater. Sci. **162**, 277 (2019).

[49] J. Yang, S. Fang, Y. Peng, S. Liu, B. Wu, R. Quhe, S. Ding, C. Yang, J. Ma, B. Shi, L. Xu, X. Sun, G. Tian, C. Wang, J. Shi, J. Lu, and J. Yang, Layer-Dependent Giant Magnetoresistance in Two-Dimensional CrPS$_4$ Magnetic Tunnel Junctions, Phys. Rev. Appl. **16**, 024011 (2021).